J. Fluid Mech. (2003), *vol.* 479, *pp.* 39–64.
DOI: 10.1017/S0022112002003300 Printed in the United Kingdom

Propagation laws for steady curved detonations with chain-branching kinetics

By MARK SHORT[1] AND JOHN B. BDZIL[2]

[1]Theoretical and Applied Mechanics, University of Illinois, Urbana, IL 61801, USA

[2]Los Alamos National Laboratory, Los Alamos, NM 87545, USA

(Received 11 February 2002)

An extension to the theory of detonation shock dynamics is made and new propagation laws are derived for steady, near-CJ (Chapman–Jouguet), weakly curved detonations for a chain-branching reaction model having two components. The first is a thermally neutral induction stage governed by an Arrhenius reaction with a large activation energy, which terminates at a location called the transition interface, where instantaneous conversion of fuel into an intermediate species (chain radical) occurs. The second is an exothermic main reaction layer (or chain-recombination zone) having a temperature-independent reaction rate. We make an ansatz that the shock curvature is sufficiently large to have a leading-order influence on the induction zone structure, whereupon it is shown that multi-dimensional effects must necessarily be accounted for in the main reaction layer. Only for exactly cylindrical or spherical waves can such multi-dimensional effects be omitted. A requirement that the main reaction layer structure pass smoothly through a sonic plane leads to a propagation law for the detonation front: a relationship between the detonation velocity, the shock curvature and various shock arclength derivatives of the position of the transition interface.

For exactly cylindrically or spherically expanding waves, a multi-valued detonation velocity–curvature relationship is found, similar to that found previously for a state-sensitive one-step reaction. The change in this relationship is investigated as the ratio of the length of the main reaction layer to the induction layer is changed. We also discuss the implications of chain-branching reaction kinetics for the prediction of critical detonation initiation energy based on detonation-velocity curvature laws. Finally several calculations that illustrate the important effect that arclength and transverse flow variations may have on the steady propagation of non-planar detonation fronts are presented. Such variations may be important for the propagation of cellular gaseous detonation fronts and for the axial propagation of detonations in a cylindrical stick of condensed-phase explosive. We also show that the arclength variations provide a formal mechanism for the existence of steady non-planar detonation fronts having converging sections, a possibility ruled out for simple irreversible one-step reaction mechanisms where only diverging steady waves are admissible.

1. Introduction

Detonations are high-speed, shock-driven, reaction waves. Generally they propagate at the Chapman–Jouguet (CJ) velocity D_{CJ} for which the reaction zone solution passes through a sonic point in a frame of reference attached to the detonation shock

(Fickett & Davis 1979). Waves that have a velocity $D_n > D_{CJ}$ possess a reaction zone solution that is subsonic throughout and rarefraction waves may continuously attenuate the detonation velocity until $D = D_{CJ}$. For $D_n < D_{CJ}$, no steady solutions are admissible (Fickett & Davis 1979). For planar detonation waves with a reaction sequence governed by simple irreversible exothermic steps, the sonic point occurs at the end of the reaction zone where the reactants are fully consumed.

Planar Chapman–Jouguet detonation waves are seldom observed, but curved fronts are. Examples include detonations propagating axially in cylindrical sticks of high explosives (Bdzil 2000), detonations in systems that undergo an area change, detonations diffracting around corners and the local fronts of cellular detonations (Klein, Krok & Shepherd 1994). Consequently there is significant interest in understanding how the propagation speed of a detonation varies with the geometry of the non-planar front, i.e. in the derivation of intrinsic surface propagation laws for the motion of curved detonations.

One very successful approach employs rational asymptotic perturbation methods and is known as detonation shock dynamics or by its acronym DSD (Bdzil 2000). It relies on two primary assumptions: weak curvature of the detonation shock (on the scale of the inverse of a characteristic length known as the half-reaction length $l_{1/2}$); and the front dynamics slowly evolve in time (on the scale of a particle transit time through $l_{1/2}$), so that the detonation velocity is a weak perturbation from the one-dimensional steady velocity. Intrinsic evolution laws can be obtained asymptotically once a reaction model is specified, and once curvature, transverse flow, velocity and time scales are set. For curved detonations with a reaction sequence consisting of simple irreversible exothermic steps, the sonic point is now located at a point of incomplete reaction, i.e. interior to the reaction zone, and front evolution laws arise by a requirement that the reaction zone solution pass smoothly through the interior sonic point.

Much of the work on detonation shock dynamics for slowly evolving or steady waves has been conducted for simple one-step reaction mechanisms of the form

$$\text{Fuel} \rightarrow \text{Product}.$$

The rates may be either state-insensitive or state-sensitive, with the sensitivity controlled by the activation energy of the reaction. For example, for a reaction rate

$$r = k(1-\lambda)^{\nu}, \tag{1.1}$$

where k is the rate constant, $\nu < 1$ is the order of the reaction and λ is the reaction progress variable, it is found that the detonation velocity D_n depends on the shock curvature κ ($\ll 1$) in an essentially linear fashion such that

$$D_n = 1 - \alpha\kappa + O(\kappa^{1/\nu}), \tag{1.2}$$

where $\alpha\,(>0)$ is a constant that depends on an integral through the entire reaction zone structure (Stewart & Bdzil 1988*b*). In this case $\kappa > 0$, i.e. the theory holds only for diverging waves, since the governing equations can be re-arranged to show that the modified thermicity (Stewart & Bdzil 1988*b*)

$$q(\gamma - 1)r - c^2\kappa(U_n + D_n), \tag{1.3}$$

where U_n is the normal component of velocity relative to the shock, must vanish at the sonic point in order for the reaction zone solution to pass through this point

smoothly. This can only happen for $\kappa > 0$, given the heat release $q > 0$, the adiabatic exponent $\gamma > 1$, and $U_n + D_n > 0$. Also c is the frozen (isentropic) sound speed.

On the other hand, for a highly state-sensitive reaction rate of the form

$$r = \epsilon k(1-\lambda)^{\nu} \exp\left[\frac{1}{\epsilon}\left(\frac{1}{c_0^2} - \frac{1}{c^2}\right)\right], \tag{1.4}$$

where c_0 is the one-dimensional steady sound speed behind the shock, and $\epsilon \ll 1$ is the inverse activation energy, the detonation velocity–curvature relation takes the form

$$D_n^{(1)} + \frac{\alpha_2}{a\alpha_1} \ln\left[1 - a\kappa^{(1)} \exp\left(bD_n^{(1)}\right)\right] = 0, \tag{1.5}$$

where $D_n = 1 + \epsilon D_n^{(1)}$, $\kappa = \epsilon\kappa^{(1)}$ and a, b, α_1 and α_2 are order-one constants. Here the curvature and detonation velocity are related by the scale $D_n - 1 = O(\kappa) = O(\epsilon)$. The nonlinear relation (1.5) gives a multi-valued response; there is a critical value of curvature beyond which no solutions exist which pass smoothly through a sonic point.

It is important to note that for the simple rate laws (1.1) and (1.4), the detonation velocity is apparently solely a function of the weak curvature of the detonation shock to leading order. Generally, this can happen in one of two ways: either the detonation front is expanding in an exactly cylindrical or spherical fashion; or transverse flow effects, i.e. spatial variations along the arclength of the shock, turn out to have a weaker effect than curvature and thus do not contribute to the evolution law at the orders considered. We will show in the following that while the latter is true for the evolution law (1.2), under the scales for which the evolution law (1.5) is derived, transverse flow effects cannot be ignored in general and thus equation (1.5) only formally applies under the first of these conditions, i.e. in the context of exactly cylindrically or spherically expanding waves.

Little work has been conducted on propagation laws for non-planar detonations with more realistic chemical reaction pathways. Exceptions include numerical studies by Sharpe (2000*a*) for a two-step sequential reaction $A \to B$, $B \to C$, with the second reaction endothermic, and Sharpe (2000*b*) for a one-step reversible reaction. Klein (1991) has also examined an extension of detonation shock dynamics for the one-step reversible reaction. The subject of the present work is a theory of detonation shock dynamics for steadily propagating waves in systems representative of realistic chain-branching kinetics. Specifically we study a two-step chain-branching reaction sequence, a model motivated by the three-step chain-branching model previously studied by Short & Quirk (1997) and Short, Kapila & Quirk (1999). These types of models have been extensively used for the purposes of large-scale computations of detonation behaviour due to their ability to capture the essential dynamics of real chain-branching reactions, e.g. Oran & Boris (1987), Oran, Jones & Sichel (1992), Kailasanath *et al.* (1991).

Our particular model has two components: a thermally neutral chain-branching induction zone and an exothermic main reaction layer or chain-recombination layer of finite extent. We note that this mimics the actual structure of detonations not only in gaseous systems but also in condensed-phase explosives. The extent of the induction zone is controlled by a reaction rate of Arrhenius form, but no heat is released due to reaction. This mimics the fact that chain-initiation and chain-branching reactions typically liberate only a small amount of heat, while the length of the induction zone is a sensitive function of the shock state. The end of the induction zone corresponds to the point where a rapid conversion of fuel into radical species occurs as in Short

& Quirk (1997). The reaction rate in the exothermic chain-recombination or main reaction layer is taken to be independent of temperature, typical of many chain-termination reactions. The ratio of the length of the induction layer to the main reaction layer is controlled by the rate constant in the main reaction layer, and plays the role of the chain-branching cross-over temperature in Short & Quirk (1997). Although this model falls short of full reaction kinetics, in contrast to the classical one-step Arrhenius model it does retain some of the essential chemical dynamics of a real chain-branching reaction.

One of the major results that arises from the present study is that, in general, variations in the detonation velocity and curvature with arclength of the detonation shock cannot be neglected in highly state-sensitive systems, including the one-step reaction (1.4) (He & Clavin 1994; Klein *et al.* 1994; Yao & Stewart 1995). We show results that illustrate the difference between the propagation of exactly cylindrically or spherically propagating detonations with one step and the model two-step chain-branching reactions, and discuss the implications of chain-branching reaction kinetics for predictions of critical detonation initiation energy based on detonation-velocity curvature laws. Finally we conduct some calculations that illustrate the important effect that arclength and transverse flow variations may have on the steady propagation of non-planar detonation fronts. We also demonstrate that arclength variations provide an avenue through which a steady non-planar detonation front may have regions of negative curvature, i.e. be of a converging nature. Such regions are not possible when arclength variations are omitted.

2. Model

The motion of a steady detonation in a Cartesian system is modelled by the reactive Euler equations,

$$\nabla\cdot(\rho\boldsymbol{u})=0,\quad (\boldsymbol{u}\cdot\nabla)\boldsymbol{u}=-\frac{1}{\rho}\nabla p,\quad (\boldsymbol{u}\cdot\nabla)e+p(\boldsymbol{u}\cdot\nabla)\left(\frac{1}{\rho}\right)=0, \tag{2.1}$$

with rate equations

$$(\boldsymbol{u}\cdot\nabla)\lambda_i=r_i, \tag{2.2}$$

for density ρ, pressure p, velocity $\boldsymbol{u}$, specific internal energy e and reaction progress variable for the ith reaction λ_i. These are augmented by the equations of state,

$$T=c^2=\frac{\gamma p}{\rho},\quad e=\frac{p}{(\gamma-1)\rho}-\sum q_i\lambda_i, \tag{2.3}$$

where c is the sound speed, T is the temperature, γ the adiabatic exponent and q_i the heat release for the ith reaction. Density has been scaled with the quiescent upstream density $\tilde{\rho}$, velocity with the steady one-dimensional Chapman–Jouguet velocity $\tilde{D}_{CJ}$, temperature with $\tilde{D}_{CJ}^2$, and pressure with $\tilde{\rho}\tilde{D}_{CJ}^2$. The heat release q_i is scaled with $\tilde{D}_{CJ}^2$, while the length scale is taken as the one-dimensional steady induction zone length, defined below. For gaseous systems $\gamma<5/3$, while it is assumed that for solid explosives $\gamma\sim 3$.

The detonation structure is determined by specification of the reaction rate kinetics. As in Short (2001), a two-step chain-branching reaction model is employed having two components: a thermally neutral chain-branching induction zone and an exothermic main reaction layer (or chain-recombination layer) of finite extent, as shown in

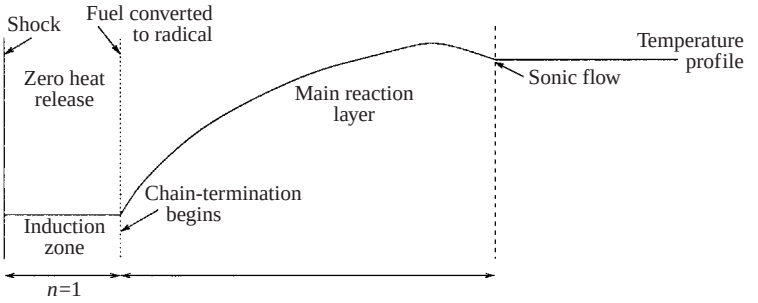

FIGURE 1. A schematic of the steady detonation structure for the two-step chain-branching reaction model.

figure 1. The rate equations may be written in the form

$$(\boldsymbol{u}\cdot\nabla)\lambda_1 = H(1-\lambda_1)r_1, \quad (\boldsymbol{u}\cdot\nabla)\lambda_2 = (1-H(1-\lambda_1))r_2, \tag{2.4}$$

where λ_1 and λ_2 are the reaction progress variables in the induction and main reaction layers respectively and $H(\ )$ is the usual Heaviside function.

2.1. *Induction zone reaction rate*

The induction zone dynamics are controlled by a reaction rate of Arrhenius form in which no heat is released due to reaction. This mimics the property that chain-initiation and chain-branching reactions typically liberate only a small amount of heat. Therefore, in the induction zone $q_1 = 0$, and

$$r_1 = k_1 \exp\left[\frac{1}{\epsilon}\left(\frac{1}{c_0^2} - \frac{1}{c^2}\right)\right], \tag{2.5}$$

where c_0 is the one-dimensional steady sound speed at the shock, k_1 is a rate constant and ϵ is the inverse activation energy, assumed small, so that

$$\epsilon \ll 1. \tag{2.6}$$

Based on the scaling that the one-dimensional steady induction zone length is unity, the rate constant k_1 is set accordingly to

$$k_1 = -U_{n0}, \tag{2.7}$$

where U_{n0} is the one-dimensional steady velocity at the shock. At the shock $\lambda_1 = 0$, while the termination of the induction zone is signalled when $\lambda_1 = 1$, where fuel is instantaneously converted into chain-radical.

2.2. *Main heat release layer reaction rate*

The reaction rate in the exothermic chain-recombination layer ($q_2 = O(1) > 0$) is assumed to be independent of the local thermodynamic state, a reasonable model for chain-termination reactions. A reaction rate of the well-known form

$$r_2 = k(1-\lambda_2)^{\nu} \tag{2.8}$$

is assumed, where k is the rate constant. The size of k then determines the ratio of the length of the chain-recombination layer (main reaction layer) to the induction zone layer. For $k = O(1)$, the two layers of are similar size, while for $k \ll 1$, the chain-recombination layer is much longer than the induction zone layer. Also, $\lambda_2 = 0$

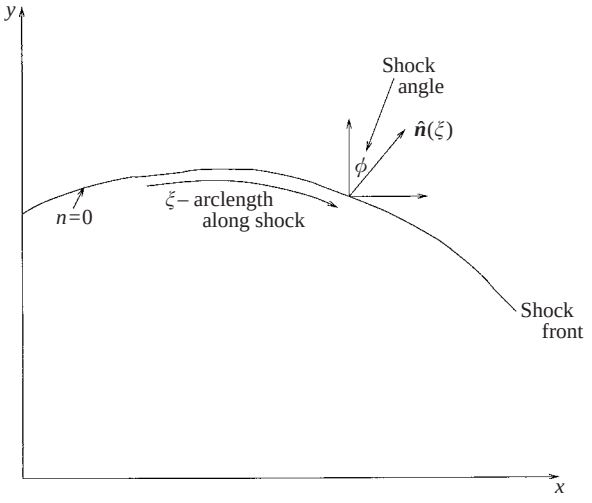

FIGURE 2. A schematic of a curved detonation shock propagating along its normal with local velocity $D_n(\xi)$ and curvature $\kappa = \phi_{,\xi}$.

marks the start of the main heat release layer, beyond which chain recombination of the chain radical occurs and heat is released, while $\lambda_2 = 1$ signals the rear equilibrium state of the detonation. The parameter ν is the order of reaction. In the following we take $\nu = 1/2$, a choice which negates the need to consider a separate transonic layer analysis (Stewart & Bdzil 1988*a*, *b*; Klein & Stewart 1993). Situations for which $1/2 < \nu \leqslant 1$ will be considered in the future.

2.3. *Bertrand-intrinsic coordinates*

To study the steady propagation of curved detonations, it is convenient to transform to a system of shock-attached coordinates (see Stewart & Bdzil 1988*b* and Yao & Stewart 1996 for a detailed description of the coordinate system employed). We use the Bertrand-intrinsic system, defined by a normal $\hat{\boldsymbol{n}}$ pointing towards the unreacted material (figure 2). The coordinate system is defined by lines instantaneously normal to the shock surface along which the non-dimensional normal distance n to the shock is measured, and by the transverse non-dimensional arclength along the shock $\bar{\xi}$. Barred quantities represent non-dimensional, but as yet unscaled variables. We use D_n to denote the normal detonation velocity, U_n the normal flow velocity relative to the shock, and u_ξ the transverse flow velocity. In this frame, the shock curvature is defined as the derivative of the shock angle $\bar{\phi}$ (the angle, as a function of $\bar{\xi}$, between the normal propagation direction of the curved shock and the direction in which the one-dimensional planar wave would move) with respect to the arclength $\bar{\xi}$. The full reactive Euler equations in this system are given in the Appendix.

2.4. *Transverse flow and curvature scalings*

Detonation shock dynamics involves subscale modelling for the propagation of curved detonation waves. It is based on two main assumptions: (i) weak curvature of the detonation shock; and (ii) the front dynamics slowly evolving in time, so that the detonation velocity is a weak perturbation from the one-dimensional steady velocity. Intrinsic evolution laws can be obtained asymptotically once curvature, velocity and time scales are set. Therein lies one of the major difficulties with the theory of

detonation shock dynamics: for a given reaction mechanism how are these scales related, and how do the scales, and consequently the form of intrinsic evolution equation, vary with changes in reaction mechanisms (Bdzil 2000)?

On the assumption that we seek an asymptotic solution for weak curvature, we may propose general scales for the shock angle $\bar{\phi}$ and arclength $\bar{\xi}$ as

$$\bar{\phi} = O(\omega) \ll 1, \quad \bar{\xi} = 1/O(\mu) \gg 1, \tag{2.9}$$

so that the curvature has size

$$\bar{\kappa} = \frac{\partial \bar{\phi}}{\partial \bar{\xi}} = O(\omega\mu) \ll 1. \tag{2.10}$$

Assuming the detonation velocity remains close to its one-dimensional steady value, we can define the detonation velocity expansion

$$D_n = 1 + O(D_n'), \quad D_n' \ll 1. \tag{2.11}$$

One relation between these three scales is provided by the geometric compatibility conditions,

$$\bar{B}\frac{\partial \bar{\phi}}{\partial \bar{\xi}} = -\frac{\partial D_n}{\partial \bar{\xi}}, \quad \frac{\partial \bar{B}}{\partial \bar{\xi}} = \bar{\kappa} D_n, \tag{2.12a, b}$$

where B is a quantity that represents the instantaneous rate of change of arclength along the shock. Given (2.9)–(2.11), (2.12b) implies $\bar{B} = O(\omega)$, from which it follows that $\bar{B}(\partial\bar{\phi}/\partial\bar{\xi}) = O(\omega^2\mu)$ and $\partial D_n/\partial\bar{\xi} = O(\mu D_n')$. Then the compatibility condition (2.12a) specifies that the shock angle scaling ω should be of the order of the square root of the velocity perturbation scale D_n', or $D_n' = O(\omega^2)$. Finally, the relation between ω and μ, which determines the curvature, must be determined by the physics one desires to capture in the intrinsic evolution law. For instance, two physically important scalings include the cases where the shock curvature is sufficiently large that it has a leading-order influence on the induction zone structure behind the shock in a curved detonation wave, or alternatively, the shock curvature is sufficiently weak that the induction zone is quasi-one-dimensional. For each of these choices, the influence of curvature on the detonation structure is then determined by the ratio of the lengths of the chain-induction to chain-branching zones.

With the above general scalings, one can define a set of $O(1)$ scaled variables,

$$\phi = \frac{\bar{\phi}}{\omega}, \quad \xi = \mu\bar{\xi}, \quad \kappa = \frac{\bar{\kappa}}{\omega\mu}, \quad B = \frac{\bar{B}}{\omega}, \tag{2.13}$$

leading to the representation of equations (2.1)–(2.4) in the Bertrand-intrinsic system given in the Appendix. Note that the transverse momentum equation shows

$$\bar{u}_\xi = O(\mu), \tag{2.14}$$

from which an $O(1)$ transverse velocity may be defined,

$$u_\xi = \bar{u}_\xi/\mu. \tag{2.15}$$

For the model reaction scheme under investigation, we anticipate that deviations of the detonation velocity D_n from its one-dimensional value will be of $O(\epsilon)$ based on the form of the Arrhenius reaction rate,

$$D_n = 1 + \epsilon D_n^{(1)}. \tag{2.16}$$

This specifies the shock angle scaling ω to be

$$\omega = \sqrt{\epsilon}. \tag{2.17}$$

Finally, making the ansatz that curvature of the detonation front should influence the induction zone structure (Buckmaster 1989; Klein *et al.* 1994; Yao & Stewart 1995), i.e. $\bar{\kappa} = O(\epsilon)$, then specifies the arclength scaling

$$\mu = \sqrt{\epsilon}. \tag{2.18}$$

With these scalings, the divergence of the flow that results from the curvature of the shock has a non-trivial influence on the induction zone solution (Buckmaster 1989).

2.5. *Reduced equations*

With the scalings (2.16)–(2.18) fixed, the full system of equations in the Appendix can now be simplified. Keeping only terms on the right-hand side of the mass, n-momentum and energy equations (A 1), (A 2), (A 4) that are of $O(\epsilon)$, and terms on the right-hand side of the ξ-momentum (A 3) and rate equation (A 5) that are $O(1)$, a set of reduced equations in the intrinsic frame can be written such that

mass:

$$\frac{\partial}{\partial n}(\rho U_n) = -\epsilon\kappa\rho(U_n + D_n) - \epsilon\left[\frac{\partial}{\partial \xi}(\rho u_\xi) + B\frac{\partial \rho}{\partial \xi}\right], \tag{2.19}$$

n-momentum:

$$U_n\frac{\partial U_n}{\partial n} + \frac{1}{\rho}\frac{\partial p}{\partial n} = -\epsilon(u_\xi + B)\frac{\partial U_n}{\partial \xi}, \tag{2.20}$$

ξ-momentum:

$$U_n\frac{\partial u_\xi}{\partial n} = -\frac{1}{\rho}\frac{\partial p}{\partial \xi}, \tag{2.21}$$

energy:

$$U_n\frac{\partial e}{\partial n} - \frac{p}{\rho^2}U_n\frac{\partial \rho}{\partial n} = -\epsilon(u_\xi + B)\left(\frac{\partial e}{\partial \xi} - \frac{p}{\rho^2}\frac{\partial \rho}{\partial \xi}\right), \tag{2.22}$$

reaction:

$$U_n\frac{\partial \lambda_i}{\partial n} = r_i. \tag{2.23}$$

The terms on the right-hand sides of (2.19)–(2.23) represent arclength flow variations, recalling that

$$\kappa = \kappa(\xi), \quad D_n = D_n(\xi). \tag{2.24}$$

To the order of analysis to be conducted in the following, termination of right-hand sides of (2.19)–(2.23) at the order shown will be sufficient. Note that in conservative form, the n-momentum and energy equations become

$$\frac{\partial}{\partial n}\left(p + \rho U_n^2\right) = -\epsilon\kappa\rho U_n(U_n + D_n) - U_n R_1 - \rho R_2 \tag{2.25}$$

and

$$\frac{\partial}{\partial n}\left(\frac{U_n^2}{2} + \frac{c^2}{(\gamma - 1)} - \sum q_i\lambda_i\right) = -R_2 - \frac{R_3}{U_n}, \tag{2.26}$$

where

$$R_1 = \epsilon\left[\frac{\partial}{\partial\xi}(\rho u_\xi) + B\frac{\partial\rho}{\partial\xi}\right], \quad R_2 = \epsilon(u_\xi + B)\frac{\partial U_n}{\partial\xi}, \quad R_3 = \epsilon(u_\xi + B)\left(\frac{\partial e}{\partial\xi} - \frac{p}{\rho^2}\frac{\partial\rho}{\partial\xi}\right). \tag{2.27}$$

2.6. *Shock conditions*

The relations governing the motion of the shock into a uniform ambient material in the Bertrand system are

$$\left.\begin{aligned} (U_n)_s &= -\frac{D_n}{(\gamma+1)}\left[\gamma - 1 + \frac{2\delta}{D_n^2}\right], \quad (u_\xi)_s = 0, \\ \rho_s &= (\gamma+1)\left(\gamma - 1 + \frac{2\delta}{D_n^2}\right)^{-1}, \quad p_s = \frac{1}{(\gamma+1)}\left(2D_n^2 - \frac{(\gamma-1)}{\gamma}\delta\right). \end{aligned}\right\} \tag{2.28}$$

Here the subscript s denotes the shock state, while δ is given by

$$\delta = \frac{\gamma\tilde{p}}{\tilde{\rho}\tilde{D}_{CJ}^2}, \tag{2.29}$$

where $\tilde{p}$ is the dimensional ambient upstream pressure. Note that δ can be calculated from the equation for the Chapman–Jouguet detonation velocity

$$\frac{\tilde{D}_{CJ}}{\sqrt{\gamma\tilde{p}/\tilde{\rho}}} = \sqrt{1 + Q\frac{(\gamma^2-1)}{2\gamma}} + \sqrt{Q\frac{(\gamma^2-1)}{2\gamma}}, \tag{2.30}$$

where $Q = \gamma\tilde{Q}/\tilde{c}_0^2$ is the Erpenbeck scaled heat release (Short & Stewart 1998).

3. Induction zone analysis

Based on the reaction rate (2.5) and scalings (2.16)–(2.18), we expect deviations of the detonation velocity from the Chapman–Jouguet value $D_n = 1$ to be of $O(\epsilon)$, or

$$D_n = 1 + \epsilon D_n^{(1)}, \quad \epsilon \ll 1. \tag{3.1}$$

Correspondingly the shock conditions (2.28) can be expanded to $O(\epsilon)$,

$$\rho_s = \rho_0 + \epsilon\rho_{1s}, \quad p_s = p_0 + \epsilon p_{1s}, \quad (U_n)_s = U_{n0} + \epsilon U_{n1s}, \tag{3.2}$$

where

$$\rho_0 = \frac{(\gamma+1)}{\gamma - 1 + 2\delta}, \quad p_0 = \frac{1}{(\gamma+1)}\left(2 - \frac{(\gamma-1)}{\gamma}\delta\right), \quad U_{n0} = \frac{1-\gamma-2\delta}{1+\gamma} \tag{3.3}$$

is the unperturbed shock state and

$$\rho_{1s} = \frac{4\delta(\gamma+1)}{(\gamma-1+2\delta)^2}D_n^{(1)}, \quad p_{1s} = \frac{4}{(\gamma+1)}D_n^{(1)}, \quad U_{n1s} = \frac{1+2\delta-\gamma}{(\gamma+1)}D_n^{(1)} \tag{3.4}$$

represent the $O(\epsilon)$ corrections. In the main bulk of the induction zone, we define expansions

$$\rho \sim \rho_0 + \epsilon\rho_1, \quad U_n \sim U_{n0} + \epsilon U_{n1}, \quad p \sim p_0 + \epsilon p_1, \quad e \sim e_0 + \epsilon e_1, \tag{3.5}$$

where $u_\xi = O(\epsilon)$ since $u_\xi = 0$ at $n = 0$. Since there is no heat release in the induction zone, the equations to be satisfied to $O(\epsilon)$ are

$$\frac{\partial}{\partial n}(\rho U_n) = -\epsilon\kappa\rho(U_n + D_n), \quad U_n\frac{\partial U_n}{\partial n} + \frac{1}{\rho}\frac{\partial p}{\partial n} = 0, \quad U_n\frac{\partial e}{\partial n} - \frac{p}{\rho^2}U_n\frac{\partial p}{\partial n} = 0. \tag{3.6}$$

Substituting (3.5) and solving for the $O(\epsilon)$ correction terms gives

$$\left.\begin{aligned} \rho_1 - \rho_{1s} = n\kappa\left[\frac{\rho_0 U_{n0}(1+U_{n0})}{(\gamma p_0/\rho_0 - U_{n0}^2)}\right], \quad p_1 - p_{1s} = n\kappa\left[\frac{\gamma p_0 U_{n0}(1+U_{n0})}{(\gamma p_0/\rho_0 - U_{n0}^2)}\right], \\ U_{n1} - U_{n1s} = n\kappa\left[\frac{\gamma p_0 U_{n0}(1+U_{n0})}{(\gamma p_0/\rho_0 - U_{n0}^2)}\right]. \end{aligned}\right\} \tag{3.7}$$

Thus the variation in the induction zone structure is the result of the curvature of the shock front. According to the rate equation (2.4), the induction zone progress variable λ (dropping the subscript 1) increases from zero at the shock to one at the end of the induction zone, where fuel is converted instantaneously into chain radical. Then,

$$U_{n0}\frac{\partial\lambda}{\partial n} = -U_{n0}\exp\left[\frac{1}{\epsilon}\left(\frac{1}{c_0^2} - \frac{1}{c^2}\right)\right]. \tag{3.8}$$

Substituting for $c^2 = \gamma p/\rho$, and using (3.5) to expand for p and ρ, (3.8) becomes

$$\frac{\partial\lambda}{\partial n} = -\exp\left[\frac{\gamma(\gamma-1)e_{1s}}{c_0^4}\right]\exp[an\kappa], \tag{3.9}$$

where

$$a = -2\frac{(\gamma-1)}{(\gamma+1)}\frac{1}{\tilde{\delta}}, \quad (\gamma-1)e_{1s} = \frac{p_{1s}}{\rho_0} - \frac{p_0}{\rho_0^2}\rho_{1s}, \tag{3.10}$$

and

$$\tilde{\delta} = \frac{\gamma p_0}{\rho_0} = \frac{(2\gamma - \delta(\gamma-1))(\gamma - 1 + 2\delta)}{(\gamma+1)^2}. \tag{3.11}$$

Integrating equation (3.9), subject to $\lambda = 0$ at $n = 0$, gives

$$\lambda = \exp\left[\frac{\gamma(\gamma-1)e_{1s}}{c_0^4}\right]\left[\frac{1}{a\kappa}(1 - \exp[an\kappa])\right]. \tag{3.12}$$

The end of the induction zone, the transition interface $n = N(\xi)$, is signalled when $\lambda = 1$, whereupon

$$n = N(\xi) = \frac{1}{a\kappa}\log\left[1 - a\kappa\exp\left[bD_n^{(1)}\right]\right], \tag{3.13}$$

with

$$b = -\frac{4\gamma(\gamma-1)}{\tilde{\delta}^2(\gamma+1)^2}\left(1 + \frac{\delta^2}{\gamma}\right). \tag{3.14}$$

Thus $N(\xi)$ is a nonlinear function of the shock curvature κ and the $O(\epsilon)$ detonation velocity perturbation $D_n^{(1)}$. In particular,

$$N_{,\xi} = -\frac{\kappa_{,\xi}}{\kappa}\left(N + \exp\left[bD_n^{(1)} - a\kappa N\right]\right) - \frac{b}{\kappa}D_{n,\xi}^{(1)}\exp\left[bD_n^{(1)} - a\kappa N\right] = O(1), \tag{3.15}$$

so that $O(\epsilon)$ variations in D_n lead to $O(1)$ variations in the distance between the shock and transition interface N as ξ varies along the shock. Importantly, it will turn out that this property will lead to the generation of $O(\epsilon)$ transverse flow variations in the main reaction layer that appear at the same order as terms that arise due to curvature variations.

In this context, Klein (1991) has suggested that arclength variations may need to be considered in the transonic layer of a time-varying convergent detonation having a two-step reaction model similar to that considered above. Also, Aslam, Bdzil & Hill (1998) have shown that for a state-independent reaction model, transverse flow variations play an important role in defining higher-order corrections to the linear D_n–κ propagation law (1.2).

4. Main reaction layer

4.1. *Analysis for $k = O(1)$*

We first investigate the case where the lengths of the induction zone and main heat release layer are of similar magnitude, i.e. the rate constant $k = O(1)$. To begin the analysis of the main reaction layer, a transformation to a coordinate frame based in the transition interface $n = N(\xi)$ is made, where

$$(n, \xi) \to (m, \xi), \quad m = n - N(\xi), \tag{4.1}$$

so that

$$\frac{\partial}{\partial n} \to \frac{\partial}{\partial m}, \quad \frac{\partial}{\partial \xi} \to -N_\xi\frac{\partial}{\partial m} + \frac{\partial}{\partial \xi}. \tag{4.2}$$

After transforming (2.19)–(2.22), the leading-order solution in the main reaction layer is obtained via an expansion of the form

$$\rho(m, \xi) \sim \rho^{(0)}(m) + O(\epsilon), \quad p(m, \xi) \sim p^{(0)}(m) + O(\epsilon), \quad U_n(m, \xi) \sim U_n^{(0)}(m) + O(\epsilon), \tag{4.3}$$

which satisfy

$$\frac{\partial}{\partial m}\left(\rho^{(0)}U_n^{(0)}\right) = 0, \quad \frac{\partial}{\partial m}\left(p^{(0)} + \rho^{(0)}U_n^{(0)\,2}\right) = 0, \quad \frac{\partial}{\partial m}\left(\frac{U_n^{(0)\,2}}{2} + \frac{c^{(0)\,2}}{(\gamma - 1)} - q\lambda^{(0)}\right) = 0. \tag{4.4}$$

These equations are easily identified as those of Rankine–Hugoniot form that govern the one-dimensional steady detonation solution. In particular, $\rho U_n = -1 + O(\epsilon)$. To $O(\epsilon)$, (2.19)–(2.23) become in the transformed plane:

mass:

$$\frac{\partial}{\partial m}(\rho U_n) = -\epsilon\kappa\rho(U_n + D_n) + \epsilon N_{,\xi}\frac{\partial}{\partial m}(\rho(u_\xi + B)) - \epsilon\rho\frac{\partial u_\xi}{\partial \xi}, \tag{4.5}$$

n-momentum:

$$\frac{\partial}{\partial m}\left(p+\rho U_n^2\right)=\epsilon\kappa(U_n+D_n)-\epsilon N_{,\xi}\frac{\partial u_\xi}{\partial m}+\epsilon\frac{\partial u_\xi}{\partial \xi}, \tag{4.6}$$

ξ-momentum:

$$\frac{\partial u_\xi}{\partial m}=-N_{,\xi}\frac{\partial U_n}{\partial m}, \tag{4.7}$$

energy:

$$\frac{\partial}{\partial m}\left(\frac{U_n^2}{2}+\frac{c^2}{(\gamma-1)}-q\lambda\right)=\epsilon N_{,\xi}(u_\xi+B)\frac{\partial U_n}{\partial m}, \tag{4.8}$$

reaction progress:

$$\frac{\partial \lambda}{\partial m}=\frac{r}{U_n}, \tag{4.9}$$

where (4.4) has been used in simplifying the $O(\epsilon)$ expressions on the right-hand sides, and the subscript 2 has been dropped from the reaction progress variable λ and the reaction rate r. There are three types of terms that contribute to the right-hand sides. The first are those that involve modifications of the main reaction layer structure due to the curvature κ of the shock. The second are those that involve the term $N_{,\xi}$, and represent modifications of the main reaction layer structure due to the variation of the position of the transition interface with arclength, where $N_{,\xi}=O(1)$. The third are those that involve $u_{,\xi}$, the transverse flow variations induced by streamline deflection at $n=N$.

To facilitate the integration of these equations, it is convenient to transform to the reaction progress variable coordinate system, i.e. from (m,ξ) to (λ,ξ), where $\lambda=0$ corresponds to $m=0$ or $n=N(\xi)$. The transverse momentum equation (4.7) can be integrated to give

$$u_\xi=-N_{,\xi}\,(U_n-U_{n0}). \tag{4.10}$$

Using (4.10), the mass, momentum and energy equations (4.5), (4.6), (4.8) then integrate to

$$\rho U_n=\rho_N U_{nN}+\epsilon\kappa\int_0^\lambda\frac{1}{r}(U_n+D_n)\,d\lambda-\epsilon N_{,\xi}^2[\rho(U_n-U_{n0})] +\epsilon N_{,\xi}B(\rho-\rho_0)-\epsilon N_{,\xi\xi}\int_0^\lambda\frac{U_n-U_{n0}}{r}\,\mathrm{d}\lambda, \tag{4.11}$$

$$p+\rho U_n^2=p_N+\rho_N U_{nN}^2+\epsilon\kappa\int_0^\lambda\frac{U_n}{r}(U_n+D_n)\,\mathrm{d}\lambda +\epsilon N_{,\xi}^2(U_n-U_{n0})-\epsilon N_{,\xi\xi}\int_0^\lambda\frac{U_n}{r}(U_n-U_{n0})\,\mathrm{d}\lambda, \tag{4.12}$$

$$\frac{U_n^2}{2}+\frac{c^2}{\gamma-1}-q\lambda=\frac{U_{nN}^2}{2}+\frac{c_N^2}{\gamma-1}-\epsilon\frac{N_{,\xi}^2}{2}(U_n-U_{n0})^2+\epsilon N_{,\xi}B\,(U_n-U_{n0}), \tag{4.13}$$

where the subscript N denotes the state at $\lambda=0$, or $n=N(\xi)$. A perturbation solution may now be found in the form

$$\rho\sim\rho^{(0)}+\epsilon\rho^{(1)},\quad p\sim p^{(0)}+\epsilon p^{(1)},\quad U_n\sim U_n^{(0)}+\epsilon U_n^{(1)}. \tag{4.14}$$

The leading-order solution is simply the Rankine–Hugoniot relations for the one-dimensional Chapman–Jouguet wave, given by

$$\left.\begin{aligned} U_n^{(0)} &= -\frac{\gamma - l}{\gamma + 1} - \delta\frac{1 + l}{\gamma + 1}, \quad \rho^{(0)} = \frac{\gamma + 1}{\gamma - l + \delta(1 + l)}, \\ p^{(0)} &= \frac{1 + l}{\gamma + 1} + \frac{\delta}{\gamma + 1}\left(\frac{1}{\gamma} - l\right), \end{aligned}\right\} \tag{4.15}$$

where

$$l = (1 - \lambda)^{1/2}. \tag{4.16}$$

For Chapman–Jouguet waves, the parameter δ (2.29) is related to the heat release q via the expression

$$\delta = 1 - \sqrt{2q(\gamma^2 - 1)} > 0. \tag{4.17}$$

Also, the sonic parameter

$$\eta = \left[U_n^{(0)}\right]^2 - \frac{\gamma p^{(0)}}{\rho^{(0)}} \to 0 \tag{4.18}$$

as $\lambda \to 1$, indicating the sonic nature of the equilibrium flow in the Chapman–Jouguet wave.

The solution of the first-order problem $\boldsymbol{y} = [\rho^{(1)}, U_n^{(1)}, p^{(1)}]^{\mathrm{T}}$ may be written in matrix form

$$\boldsymbol{A} \cdot \boldsymbol{y} = \boldsymbol{b} = \boldsymbol{b}_0 + BN_{,\xi}\boldsymbol{b}_1 + N_{,\xi}^2\boldsymbol{b}_2 + N_{,\xi\xi}\boldsymbol{b}_3, \tag{4.19}$$

where

$$\boldsymbol{A} = \begin{bmatrix} U_n^{(0)} & \rho^{(0)} & 0 \\ \left[U_n^{(0)}\right]^2 & 2U_n^{(0)}\rho^{(0)} & 1 \\ -\dfrac{\gamma p^{(0)}}{(\gamma - 1)\left[\rho^{(0)}\right]^2} & U_n^{(0)} & \dfrac{\gamma}{(\gamma - 1)\rho^{(0)}} \end{bmatrix}, \tag{4.20}$$

$$\boldsymbol{b}_0 = \begin{bmatrix} U_{n0}\rho_N^{(1)} + \rho_0 U_{nN}^{(1)} + \kappa\displaystyle\int_0^\lambda \frac{1}{r}\left(U_n^{(0)} + 1\right)\mathrm{d}\lambda \\ p_N^{(1)} + U_{n0}^2\rho_N^{(1)} - 2U_{nN}^{(1)} + \kappa\displaystyle\int_0^\lambda \frac{U_n^{(0)}}{r}\left(U_n^{(0)} + 1\right)\mathrm{d}\lambda \\ U_{n0}U_{nN}^{(1)} + \dfrac{\gamma}{(\gamma - 1)\rho_0}p_N^{(1)} - \dfrac{\gamma p_0}{(\gamma - 1)\rho_0^2}\rho_N^{(1)} \end{bmatrix}, \tag{4.21}$$

$$\boldsymbol{b}_1 = \begin{bmatrix} \rho^{(0)} - \rho_0 \\ 0 \\ \left(U_n^{(0)} - U_{n0}\right) \end{bmatrix}, \quad \boldsymbol{b}_2 = \begin{bmatrix} -\rho^{(0)}\left(U_n^{(0)} - U_{n0}\right) \\ \left(U_n^{(0)} - U_{n0}\right) \\ -\dfrac{1}{2}\left(U_n^{(0)} - U_{n0}\right)^2 \end{bmatrix}, \tag{4.22}$$

$$\boldsymbol{b}_3 = \begin{bmatrix} -\displaystyle\int_0^\lambda \frac{U_n^{(0)} - U_{n0}}{r}\mathrm{d}\lambda \\ -\displaystyle\int_0^\lambda \frac{U_n^{(0)}}{r}\left(U_n^{(0)} - U_{n0}\right)\mathrm{d}\lambda \\ 0 \end{bmatrix}. \tag{4.23}$$

The inverse of $\boldsymbol{A}$ is given by

$$\boldsymbol{A}^{-1} = \frac{(\gamma-1)}{\eta}\begin{bmatrix} U_n^{(0)}\dfrac{(\gamma+1)}{(\gamma-1)} & -\dfrac{\gamma}{(\gamma-1)} & \rho^{(0)} \\ -\dfrac{\gamma\left(\left[U_n^{(0)}\right]^2+p^{(0)}/\rho^{(0)}\right)}{(\gamma-1)\rho^{(0)}} & \dfrac{U_n^{(0)}\gamma}{(\gamma-1)\rho^{(0)}} & -U_n^{(0)} \\ U_n^{(0)}\left(\left[U_n^{(0)}\right]^2+\dfrac{2\gamma}{(\gamma-1)}\dfrac{p^{(0)}}{\rho^{(0)}}\right) & -\left(\left[U_n^{(0)}\right]^2+\dfrac{\gamma}{(\gamma-1)}\dfrac{p^{(0)}}{\rho^{(0)}}\right) & \left[U_n^{(0)}\right]^2\rho^{(0)} \end{bmatrix}, \tag{4.24}$$

which is singular as $\lambda \to 1$, where $\eta \to 0$. In order to invert the relation (4.19), a regularization condition must be invoked, which amounts to setting any line of the matrix $\boldsymbol{A}^{-1}\cdot\boldsymbol{b} = 0$ at $\lambda = 1$. The result is a propagation law for the motion of the detonation front: a relationship between the detonation velocity $D_n^{(1)}$, the curvature κ and various arclength derivatives of the transition interface N, given by

$$\alpha_1 D_n^{(1)} + \alpha_2 N\kappa + \alpha_3\kappa + \alpha_4 B N_{,\xi} + \alpha_5 N_{,\xi}^2 + \alpha_6 N_{,\xi\xi} = 0, \tag{4.25}$$

where

$$\alpha_1 = -\frac{(1-\delta^2)}{(\gamma-1)(\gamma+\delta)}, \quad \alpha_2 = \frac{(2\gamma-(\gamma-1)\delta)(1-\delta)}{(\gamma-1)(\gamma+1)((\gamma-1)+2\delta)} \tag{4.26}$$

$$\alpha_3 = -\frac{3}{k}\frac{(1-\delta)}{(\gamma+1)(\gamma-1)}\left(\delta+\frac{14\gamma(1-\delta)}{9(\gamma+1)}\right), \quad \alpha_4 = \frac{(1-\delta)(3\gamma-1-(\gamma-3)\delta)}{(\gamma-1)(\gamma-1+2\delta)(\gamma+\delta)} \tag{4.27}$$

$$\alpha_5 = -\frac{(1-\delta)(3\gamma-1-(\gamma-3)\delta)}{2(\gamma-1)(\gamma+1)(\gamma+\delta)}, \quad \alpha_6 = -\frac{(1-\delta)}{3k(\gamma+1)^2(\gamma-1)}(4\gamma-(\gamma-3)\delta). \tag{4.28}$$

It is easily demonstrated that $\alpha_1 < 0$, $\alpha_2 > 0$, $\alpha_3 < 0$, $\alpha_4 > 0$, $\alpha_5 < 0$, $\alpha_6 < 0$.

The evolution law (4.25) has been derived assuming a geometry that allows for two-dimensional flow variations. When the detonation wave is perfectly cylindrically or spherically expanding, transverse flow derivatives are zero, and (4.25) reduces to

$$D_n^{(1)} + \frac{\alpha_2}{a\alpha_1}\ln\left[1-a\kappa\exp\left(bD_n^{(1)}\right)\right] + \frac{\alpha_3}{\alpha_1}\kappa = 0, \tag{4.29}$$

a relation between the detonation velocity $D_n^{(1)}$ and the curvature κ.

Before proceding, an important implication of the role of transverse derivatives can be seen by combining (4.5)–(4.9) in the form of a 'Master' equation (Bdzil 1981),

$$\left[c^2\left(1+\epsilon N_{,\xi}^2+\epsilon\frac{N_{,\xi}}{U_n}(u_\xi+B)\right)-U_n^2\left(1-\epsilon\frac{N_{,\xi}}{U_n}(u_\xi+B)\right)\right]\frac{\partial U_n}{\partial m} = (\gamma-1)qr-\epsilon c^2\kappa(U_n+D_n)+\epsilon c^2 N_{,\xi\xi}(U_n-U_{n0}). \tag{4.30}$$

This shows that for the main reaction layer solution to pass through a point where the coefficient of $\partial U_n/\partial m$ vanishes, the right-hand side of (4.30) must be zero at that point. In the absence of arclength variations, this restricts quasi-steady solutions

to diverging waves where $\kappa > 0$, since $(\gamma - 1)qr > 0$. When arclength variations are included no such restriction is present. In particular, for converging waves where $\kappa < 0$, the right-hand side can still vanish provided $N_{,\xi\xi} > 0$, where $U_n - U_{n0} < 0$. Arclength variations provide a way in which regions of quasi-steady converging detonation fronts may exist. Such situations are demonstrated below.

4.2. *Analysis for* $k \gg 1$

The evolution equation (4.25) has been derived assuming that the rate constant in the main reaction layer $k = O(1)$, i.e. for the case where the length of the main reaction layer is of the order of the induction zone. However, when the rate constant $k \gg 1$, the length of the main reaction layer is smaller than that of the induction zone layer. In the limit $k \to \infty$, the main reaction layer becomes a jump discontinuity. The corresponding evolution equation for the detonation front can be derived in a similar manner to that above. For formal bookkeeping purposes, suppose $k = O(1/\sqrt{\epsilon})$. Defining

$$\bar{k} = \sqrt{\epsilon} k, \tag{4.31}$$

the rate equation (4.9) suggests a rescaling of the form

$$m = \sqrt{\epsilon}\bar{m}. \tag{4.32}$$

The mass, momentum and energy equations (4.5), (4.6) and (4.8) indicate that the only terms that survive at $O(\epsilon)$ on the right-hand sides are those that involve the partial m derivatives. A perturbation analysis leads to the evolution equation

$$\alpha_1 D_n^{(1)} + \alpha_2 N\kappa + \alpha_4 B N_{,\xi} + \alpha_5 N_{,\xi}^2 = 0, \tag{4.33}$$

which is precisely the equation obtained from (4.25) in the limit $k \gg 1$, where $\alpha_1, \alpha_6 \to 0$. For cylindrically curved waves (4.33) becomes

$$D_n^{(1)} + \frac{\alpha_2}{a\alpha_1} \ln\left[1 - a\kappa \exp\left(bD_n^{(1)}\right)\right] = 0, \tag{4.34}$$

which has the same form as that previously obtained by Yao & Stewart (1995), Klein *et al.* (1994) and He & Clavin (1994). It has been shown here to apply only to cylindrically symmetric waves and thin main reaction layers.

4.3. *Analysis for* $k \ll 1$

When the rate constant $k \ll 1$, the length of the main reaction layer is larger than that of the induction zone layer. For bookkeeping purposes, suppose $k = O(\sqrt{\epsilon})$. Defining

$$\bar{k} = k/\sqrt{\epsilon}, \tag{4.35}$$

the rate equation (4.9) suggests a rescaling of the form

$$m = \bar{m}/\sqrt{\epsilon}. \tag{4.36}$$

The mass (4.5), momentum (4.6), ξ-momentum (4.7), and energy (4.8) equations then become

mass:

$$\frac{\partial}{\partial \bar{m}}(\rho U_n) = -\sqrt{\epsilon}\kappa\rho(U_n + D_n) - \sqrt{\epsilon}\rho\frac{\partial u_\xi}{\partial \xi}, \tag{4.37}$$

n-momentum:

$$\frac{\partial}{\partial \bar{m}}\left(p + \rho U_n^2\right) = \sqrt{\epsilon}\kappa(U_n + D_n) + \sqrt{\epsilon}\frac{\partial u_\xi}{\partial \xi}, \tag{4.38}$$

ξ-momentum:

$$\frac{\partial u_\xi}{\partial \bar{m}} = -N_{,\xi}\frac{\partial U_n}{\partial \bar{m}}, \tag{4.39}$$

energy:

$$\frac{\partial}{\partial \bar{m}}\left(\frac{U_n^2}{2} + \frac{c^2}{(\gamma-1)} - q\lambda\right) = 0. \tag{4.40}$$

Thus $O(\sqrt{\epsilon})$ perturbations are generated in the main reaction layer arising from curvature terms that are $O(\sqrt{\epsilon})$ on the scale of the main reaction layer and from $O(\sqrt{\epsilon})$ transverse flow velocity perturbations that are generated by the deflection of the transition layer N. A perturbation solution may now be found in the form

$$\rho \sim \rho^{(0)} + \sqrt{\epsilon}\rho^{(1)}, \quad p \sim p^{(0)} + \sqrt{\epsilon}p^{(1)}, \; U_n \sim U_n^{(0)} + \sqrt{\epsilon}U_n^{(1)}, \tag{4.41}$$

where $\rho^{(1)} = p^{(1)} = U_n^{(1)} = 0$ at $n = N(\xi)$, since the induction zone perturbations are $O(\epsilon)$. Again, an analysis similar to that above leads an evolution equation which takes the form

$$\bar{\alpha}_3\kappa + \bar{\alpha}_6 N_{,\xi\xi} = 0, \tag{4.42}$$

where $\bar{\alpha}_3 = k\alpha_3$ and $\bar{\alpha}_6 = k\alpha_6$. This is precisely the equation obtained through (4.25) for any $k \ll 1$, where $\alpha_1, \alpha_6 \gg 1$.

Equations (4.25), (4.29), (4.33), (4.34) and (4.42) represent various forms and limits of detonation front evolution equations for the two-step chain-branching reaction model presented in § 2. Below we investigate the properties of these equations and their implications for detonation initiation studies.

5. Cylindrically and spherically curved waves

The evolution equations for $k = O(1)$, (4.29), and for $k \gg 1$, (4.34), represent detonation velocity–curvature laws for exactly cylindrically or spherically expanding waves. We emphasize that this is the only circumstance in which arclength variations can generally be ignored for highly state-sensitive reactions. Equation (4.29) is a generalization of the previously derived (4.34) (Yao & Stewart 1995; He & Clavin 1994; Klein *et al.* 1994), which now accounts for the presence of a main reaction layer of finite extent.

The difference between (4.29) and (4.34) can be interpreted in the context of the three-step chain-branching reaction model studied in Short & Quirk (1997). Here the ratio of the length of the chain-induction to chain-termination regions is set by the chain-branching cross-over temperature T_B. When T_B is sufficiently close to a given detonation shock temperature, the chain-induction zone is dominant and the main reaction layer can legitimately be replaced by a discontinuous heat release region (the classical square-wave). This structure relates to the limit $k \gg 1$ above, (4.34). As T_B is reduced, the chain-induction region shrinks, and the structure of the chain-branching region must be included. We have derived a modified detonation velocity–curvature law (4.29) for cylindrically or spherically expanding waves that accounts for the presence of a finite region of heat release.

For given characteristic detonation parameter values, (4.29) and (4.34) lead to multi-valued detonation velocity–curvature responses. A critical value of curvature κ_c exists beyond which no quasi-steady solution exists that has a main reaction layer structure that passes through a sonic line. Presumably, unsteady effects acting on a curved detonation that has $\kappa > \kappa_c$ may either attract the detonation to a steady solution having $\kappa < \kappa_c$ (or some solution that bifurcates from the branch of steady

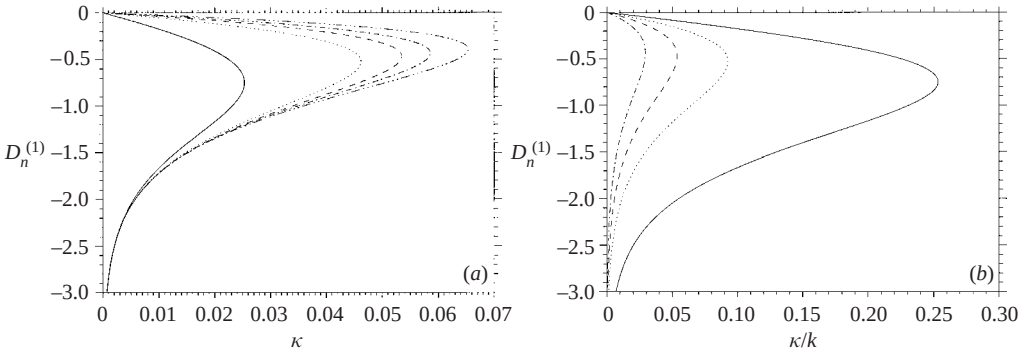

FIGURE 3. Solutions of (4.29) and (4.34): (*a*) $D_n^{(1)}$ vs. κ and (*b*) $D_n^{(1)}$ vs. κ/k for $k = \infty$ (dash-dot-dot-dot), $k = 2$ (dash-dot), $k = 1$ (dash), $k = 0.5$ (dot), $k = 0.1$ (solid). Parameters are $\delta = 0.182$ ($Q = 5$), and $\gamma = 1.2$.

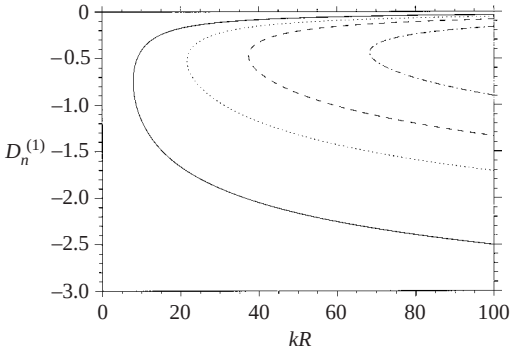

FIGURE 4. Solutions of (4.34), $D_n^{(1)}$ vs. Rk for $k = 2$ (dash-dot), $k = 1$ (dash), $k = 0.5$ (dot), $k = 0.1$ (solid). Parameters are $\delta = 0.182$ ($Q = 5$), and $\gamma = 1.2$.

solutions for $\kappa < \kappa_c$ if these are unstable), or cause continuous erosion of the shock front and hence detonation failure.

$D_n^{(1)}$–κ responses for several values of the rate constant k obtained from (4.29), and for $k = \infty$ obtained from (4.34) are shown in figure 3(*a*). Here the curvature scale is based on the inverse of the physical induction zone length. A better choice would be to base these scalings on the inverse of the physical length of the main reaction layer, since the reaction rate in this layer is independent of the thermodynamic state and thus is not likely to vary substantially between different detonation shock states. For instance, in the three-step reaction studied by Short & Quirk (1997), it is the induction zone length which varies substantially with varying cross-over temperature T_B. Figure 3(*b*) shows $D_n^{(1)}$ plotted against κ/k, where the critical curvature κ_c/k increases as k is decreased, i.e. the induction zone becomes shorter. Thus this is the response expected by decreasing T_B in Short & Quirk (1997). Figure 4 is the same but with $D_n^{(1)}$ plotted against the shock radius $R(= 2/\kappa)$ for a spherically expanding wave, scaled with the rate constant k.

He & Clavin (1994) have suggested that conditions at the critical turning point can be used to provide a critical initiation energy E_c for detonation. Their idea is to replace the shock radius and velocity in the self-similar blast wave initiation energy formula (Taylor 1950) by those at the critical turning point in the above quasi-steady

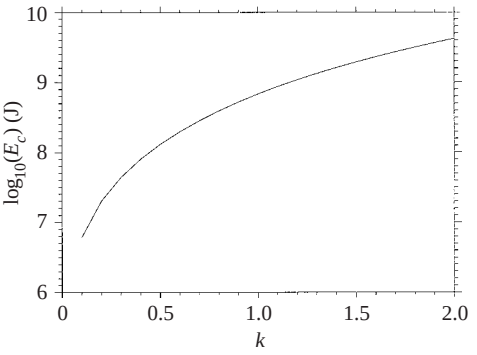

FIGURE 5. Variation of the critical initiation energy E_c (J) with rate constant k for a spherically expanding wave.

analysis, U_c and R_c, i.e.

$$E_c = A_j \left(\frac{j+3}{2} \right)^2 \rho_0 U_c^2 R_c^{j+1}, \tag{5.1}$$

where $j = 1$ for cylindrical waves and $j = 2$ for spherical waves. This is on the basis that the supplied initiation energy must induce a shock of sufficient radius that exceeds the critical shock radius R_c for a detonation to result. The energy integral constant A_j is given by Korobenikov (1991):

$$A_2 = 0.31246(\gamma - 1)^{-1.1409 - 0.11735 \log_{10}(\gamma - 1)} \tag{5.2}$$

for a spherical wave (Eckett, Quirk & Shepherd 2000). Thus figure 4 also shows the variation in critical shock radius for various ratios of induction layer size to main reaction layer size defined by k. Thus if the extent of the main reaction layer is fixed, a smaller critical shock radius results as the extent of the induction zone decreases (or T_B decreases in the model of Short & Quirk (1997), a conclusion that has been verified recently by direct numerical simulation (Short, Sharpe & Bdzil 2001).

Figure 5 shows how the critical initiation energy (5.1) would vary with rate constant k, for a detonation which runs at a one-dimensional steady Chapman–Jouguet velocity of $1800\,\mathrm{m\,s^{-1}}$, initial density $\rho_0 = 1.1741\,\mathrm{kg\,m^{-3}}$, $\gamma = 1.2$ and $\epsilon = 1/14$, in which the main reaction layer extent is kept fixed at 5×10^{-3} m. Consequently, in the context of the three-step model (Short & Quirk 1997), the energy required to initiate a detonation would increase as the chain-branching cross-over temperature increased, a trend also verified in Short *et al.* (2001).

Direct numerical simulation calculations of detonation initiation, using the current two-step reaction model will be presented in a future article to ascertain the accuracy of the initiation energy trends predicted by the above asymptotic model for a detonation with separate induction and main reaction layers. It should also be noted that some recent studies have argued that quantitatively accurate predictions of critical initiation energies should incorporate unsteady effects (Lee & Higgins 1999; Eckett, *et al.* 2000). Extensions of the current steady analysis to include unsteadiness, arclength variations and the effects of separate induction and main reaction zone layers will also be considered in a future article. However, it should be noted that Short *et al.* (2001) have found that for initiation studies based on the three-step chain-branching model, the notion that one can predict criticality based on the critical curvature point

associated with a steady analysis remains a valid one for both stable and unstable detonation waves for that particular reaction model.

6. Steady curved waves with arclength variations

We have demonstrated that for a detonation propagating in a mixture that has a high degree of state sensitivity, variations of the shock curvature and velocity with arclength cannot be ignored in general. Two situations where such variations may be important are the cellular structures observed in gaseous detonations and the axial propagation of a steady curved detonation in a cylindrical stick of high explosive (also known as a rate-stick (Bdzil 1981)).

Detonations propagating in gaseous explosives are nearly always observed to have a cellular nature, consisting of time-varying, weakly curved, periodic bulges of the shock front, separated by Mach stems, which arise due to a multi-dimensional instability of the planar detonation front (Fickett & Davis 1979). Two-dimensional numerical calculations of cellular detonations (e.g. Bourlioux & Majda 1992; Sharpe & Falle 2000; Sharpe 2001) appear to indicate non-trivial variations of the shock curvature with arclength in these periodic sections. Although cellular detonations are time-evolving structures, typical cell widths can be of the order of one hundred times longer than the one-dimensional reaction zone thickness, and so it is important to realize that cellular detonations evolve in a slowly varying fashion. Consequently, it seems reasonable to ask if the steady solutions predicted for example by (4.25) will be an important factor in the evolution of cellular detonations, in which time-varying effects could be incorporated in a consistent perturbative manner. Indeed, this is the strategy adopted by Yao & Stewart (1996) in deriving a detonation cell evolution equation, one which does not take into account arclength variations.

For a detonation propagating axially in a cylindrical stick of high explosive, the speed of propagation of the wave is determined by conditions at the stick edge. Typically the rate stick is encased in an inert metallic material and the properties of this material determine how the combustion products may expand at the edge, i.e. the liner provides a confinement effect. Boundary conditions to be satisfied at the edge are then determined by specifying information about the shape of the streamlines there. For state-sensitive systems, the propagation of a detonation in a rate stick must include variations in curvature and velocity with arclength along the detonation shock.

Given this information, we will now examine some possible steady solutions of the new evolution law (4.25) related to the two problems discussed above. The calculations presented below are by no means exhaustive, due to the extensive parameter space that would need to be explored in general, but are representative of the behaviour one may expect to observe. More extensive studies of the steady solutions of (4.25) will be presented in a future article.

We assume a detonation that propagates with a constant velocity D_a in the axial direction in a rate stick or rectangular shock tube. Then at every point along the detonation shock the detonation velocity D_n (figure 6) is

$$D_n = D_a \cos\bar{\phi}. \tag{6.1}$$

For small shock angles, we may write

$$D_n^{(1)} = D_a^{(1)} - \frac{\phi^2}{2}, \tag{6.2}$$

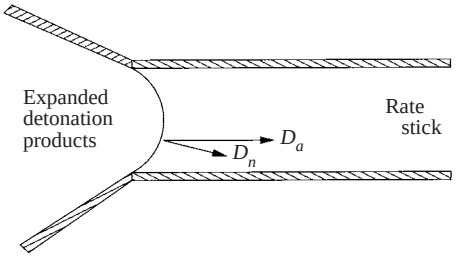

FIGURE 6. A schematic of a curved detonation shock propagating along along a rate stick.

where $D_a \sim 1 + \epsilon D_a^{(1)}$ and $D_a^{(1)}$ is a constant. Therefore,

$$D_{n,\xi}^{(1)} = -\phi\phi_{,\xi} = -\phi\kappa. \tag{6.3}$$

An equation which relates the variation of N_ξ with ξ can be obtained by re-arranging (4.25),

$$\frac{\mathrm{d}}{\mathrm{d}\xi}(N_{,\xi}) = -\frac{1}{\alpha_6}\left[\alpha_5 N_{,\xi}^2 + \alpha_4 B N_{,\xi} + \alpha_3\kappa + \alpha_2 N\kappa + \alpha_1 D_n^{(1)}\right], \tag{6.4}$$

where the B-term appearing in (6.4) can be determined from the geometric identities (2.12). Equation (2.12b) can be integrated to give

$$B \sim \phi + A, \tag{6.5}$$

for constant A. Equation (2.12a) implies $A = 0$ when compared with (6.2) Similarly, an equation which relates the variation of κ with ξ can be obtained by re-arranging (3.15),

$$\frac{\mathrm{d}\kappa}{\mathrm{d}\xi} = -\frac{\kappa}{N\left(1 - a\kappa \mathrm{e}^{bD_n^{(1)}}\right) + \mathrm{e}^{bD_n^{(1)}}}\left[\left(1 - a\kappa \mathrm{e}^{bD_n^{(1)}}\right)N_{,\xi} + bD_{n,\xi}^{(1)}\mathrm{e}^{bD_n^{(1)}}\right]. \tag{6.6}$$

Finally ϕ and κ are related by

$$\frac{\mathrm{d}\phi}{\mathrm{d}\xi} = \kappa. \tag{6.7}$$

Thus with (3.13), equations (6.4), (6.6) and (6.7) represent a set of three coupled differential equations which determine κ, D_n and N as a function of ξ when supplemented by appropriate boundary conditions. Note that (6.4), (6.6) and (6.7) are invariant under the transformation $\xi \to -\xi$, $\phi \to -\phi$. The relationship between the transverse coordinate in a Cartesian system or the radius of a rate stick r and the arclength ξ in the Bertrand system is given by

$$r_{,\xi} = \cos(\bar{\phi}), \tag{6.8}$$

so that $r \sim \xi$.

Periodic solutions to the system (6.4), (6.6) and (6.7), which could be relevant to the weakly nonlinear propagation of periodic cellular structures in gaseous mixtures slightly above marginal stability, are obtained by applying the symmetry boundary conditions

$$\phi = 0, \quad N_{,\xi} = 0, \quad D_{n,\xi}^{(1)} = 0, \quad \kappa_{,\xi} = 0 \tag{6.9}$$

at two points $\xi = 0$ and $\xi = \xi_e$. For an initial guess of the axial velocity $D_a^{(1)}$ and curvature κ at $\xi = 0$, (6.2) to (6.7) are integrated to the point $\xi = \xi_e$, and $D_a^{(1)}$ and κ at $\xi = 0$ iterated until (6.9) at $\xi = \xi_e$ is satisfied. Figure 7 shows one possible periodic

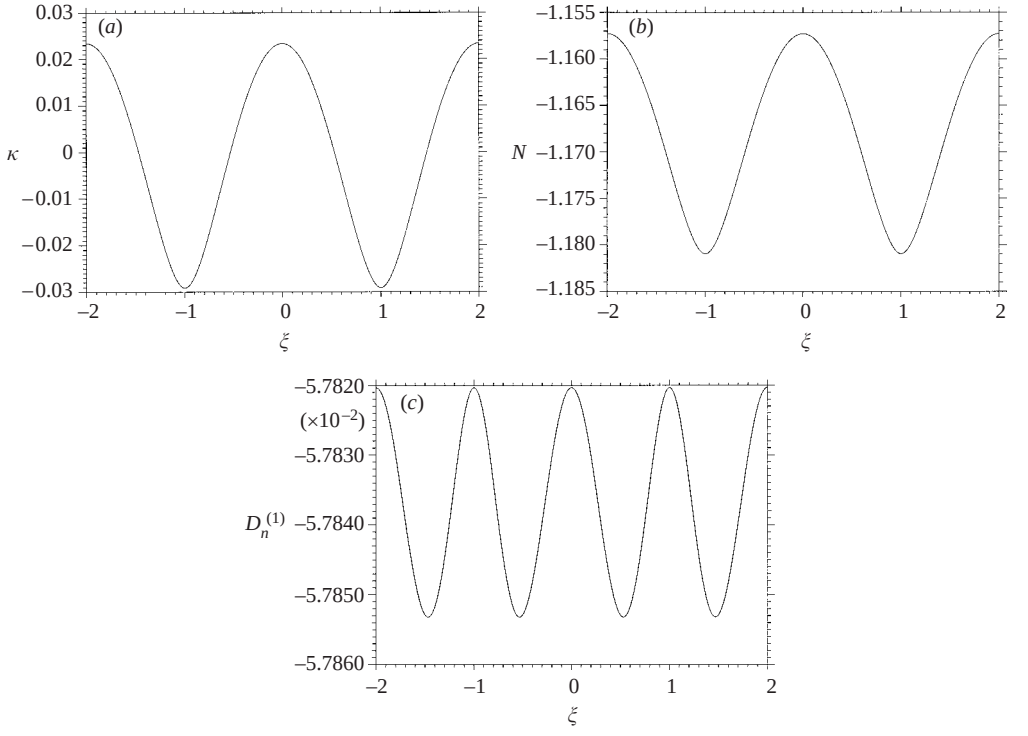

FIGURE 7. (*a*) Change in curvature with ξ along a periodically varying detonation shock front with $Q = 5$, $\gamma = 1.2$ and $k = 0.5$. The wavelength is $r \sim \xi = 2$. (*b*, *c*) Corresponding variations of N and $D_n^{(1)}$.

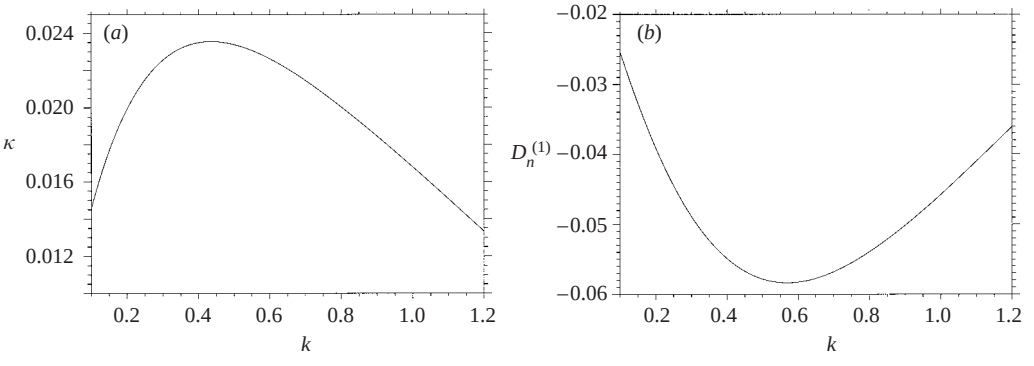

FIGURE 8. Variation of the curvature κ and velocity $D_n^{(1)}$ at $\xi = 0$ with rate constant k for a periodically varying detonation front with $Q = 5$, $\gamma = 1.2$, and wavelength $r \sim \xi = 2$.

structure obtained for $Q = 5$, $\gamma = 1.2$, and a rate constant $k = 0.5$ with $\xi_e = 1$. Of particular note in figure 7(*a*) is the marked variation and change in sign of κ with arclength ξ over a typical period. The latter represents a transition from a diverging to converging section of the shock front. Figure 7(*b*) shows the lag in the location of the transition zone N due to variations in the detonation velocity and curvature with arclength. Figure 8 shows the variation of κ and $D_n^{(1)}$ at $\xi = 0$ with rate constant k for a periodically varying detonation front with $Q = 5$, $\gamma = 1.2$ and $\xi_e = 1$.

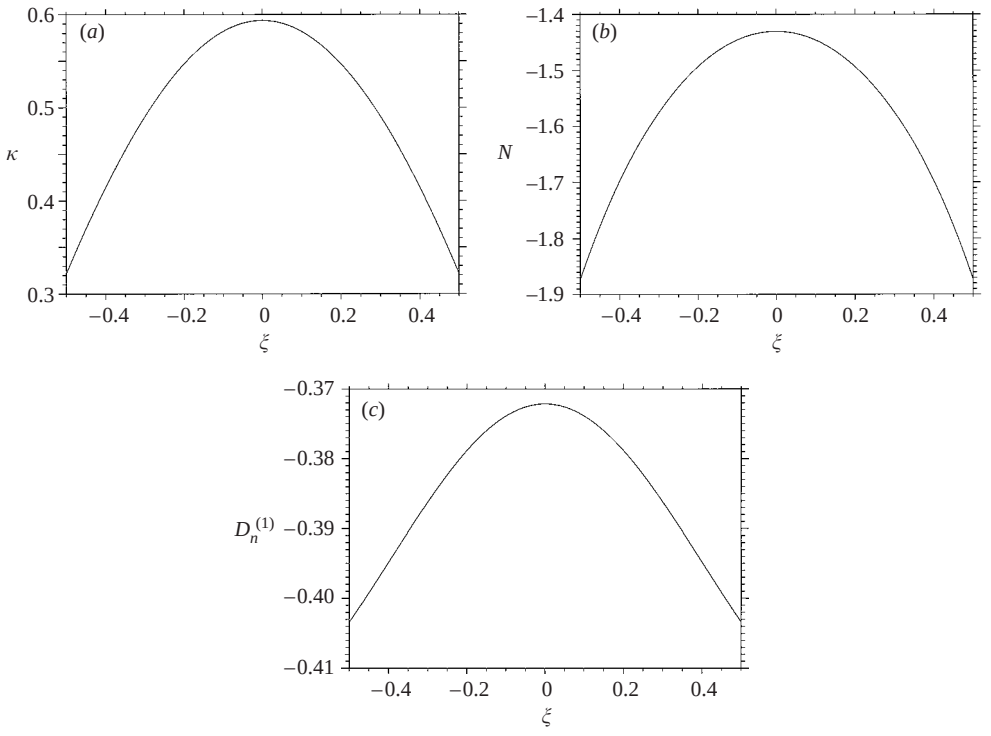

FIGURE 9. (*a*) Variation of curvature with arclength along a detonation shock propagating in a rate stick of radius $r \sim \xi = 0.5$ with edge conditions $\kappa_{,\xi} = -1$, $\phi = 0.25$ for $Q = 10$, $\gamma = 3$ and $k = 0.5$. (*b*, *c*) Corresponding variations of N and $D_n^{(1)}$.

Solutions to the rate-stick problem which account for arclength variations are obtained by applying (6.9) on the axis $\xi = 0$. Edge conditions at $\xi = \xi_e$ are determined by providing information on how the detonation front and combustion products are confined at the stick edge. We refer the reader to Stewart & Bdzil (1988*b*) and Aslam, Bdzil & Stewart (1996) for more details. For the present case, we will specify the shock angle ϕ and the gradient of curvature with arclength $\kappa_{,\xi}$, conditions that are, in principle, sufficient to specify the streamline deflection occurring at the edge of the stick for the higher-order system under study. Further research, involving a local asymptotic analysis near the edge of the rate stick, is currently being conducted in order to construct the boundary conditions that would be relevant to a particular confinement material as in Aslam *et al.* (1996). Equations (6.2) to (6.7) are then integrated from $\xi = 0$ to $\xi = \xi_e$, the stick radius, and $D_a^{(1)}$ and κ at $\xi = 0$ adjusted until the given values of $\kappa_{,\xi}$ and ϕ on the stick edge are satisfied.

Figure 9 shows one possible solution of the variation of κ, N and $D_n^{(1)}$ with arclength along a detonation shock propagating in a rate stick of radius $r \sim \xi = 0.5$ with edge conditions $\kappa_{,\xi} = -1$, $\phi = 0.25$ for $Q = 10$, $k = 0.5$, and $\gamma = 3$, chosen to represent the behaviour in a solid explosive. Again substantial variations in κ are observed in figure 9(*a*), with κ decreasing from a maximum on the stick axis to a minimum on the stick edge. Figure 9(*b*) shows the corresponding lag in the location of the transition interface N.

Of particular interest is figure 10, which shows the variation of κ and $D_n^{(1)}$ on the stick axis with rate constant k for a detonation having the parameter values defined in

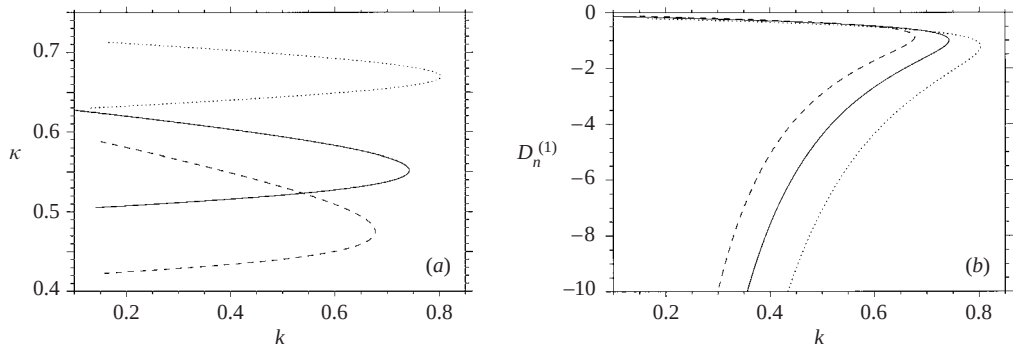

FIGURE 10. Variation of the axial curvature κ and velocity $D_n^{(1)}$ with rate constant k for a detonation in a rate stick with $Q = 10$, $\gamma = 3$, having edge conditions $\kappa_{,\xi} = -1$, $\phi = 0.25$, for three stick radii: $r \sim \xi = 0.4$ (dashed line), $r \sim \xi = 0.5$ (solid line), and $r \sim \xi = 0.6$ (dotted line).

figure 9 for three different stick radii, $r \sim \xi = 0.4,\ 0.5,\ 0.6$. They show a multi-valued response where, for a given stick radius, there are no solutions if the rate constant is too large. The upper and lower branches of figure 10(a) correspond directly to the upper and lower branches of figure 10(b). Thus if the rate constant is either too large for a given radius, i.e. the ratio of the length of the main reaction layer over the induction layer is too small, or the radius too small for a given rate constant, there are no steady solutions of the system (6.2)–(6.7). Since decreasing k corresponds to a widening of the main reaction layer relative to the induction zone, curved detonations may exist in sticks of small radii if the main reaction layer is sufficiently long. Thus detonations reacting according to the rate law (2.4) with larger rate constants need larger radii for a steady solution to exist.

7. Summary

An important extension to the theory of detonation shock dynamics has been presented for a steady, near-CJ, weakly curved detonation with a model chain-branching reaction having two components, beginning with a thermally neutral induction zone whose length is governed by an Arrhenius reaction rate with an inverse activation energy ϵ. This terminates along a curve $N(\xi)$ where conversion of fuel into an intermediate species (chain radical) occurs, which is followed by an exothermic main reaction layer or chain-recombination zone having a temperature-independent reaction rate with rate constant k. The ratio of the length of the induction zone to the main reaction layer is controlled by k. Deviations of the detonation velocity D_n from the planar steady value are $O(\epsilon)$, which sets the shock angle amplitude to be $O(\sqrt{\epsilon})$. Making the ansatz that curvature should induce an $O(\epsilon)$ flow divergence in the induction zone sets the arclength (or transverse flow) scale to be $O(1/\sqrt{\epsilon})$.

Based on these scales an analysis of the induction zone leads us to conclude that $O(\epsilon)$ variations in D_n lead to $O(1)$ variations in the distance between the shock and transition interface N as the arclength ξ varies along the shock. It is this variation that results in the generation of $O(\epsilon)$ transverse flow and arclength changes in the main reaction layer of the detonation, changes that appear at the same order as terms that arise due to the influence of shock curvature. A regularization condition arising from the near-CJ propagation speed of the detonation leads to a propagation law for

the motion of the detonation front: a relationship between the detonation velocity D_n, the shock curvature κ and various arclength derivatives of the transition interface N. It is also shown that arclength variations provide a mechanism for the theoretical existence of a converging steady non-planar detonation front. Arclength variations can only generally be ignored when the detonation is expanding in either an exactly cylindrical or spherical manner.

We have shown results that compare the variation of the detonation velocity with curvature for spherically propagating detonations with the previously studied one-step large-activation-energy system and the present model two-step chain-branching reaction. We also discuss the implications that chain-branching reaction kinetics has for predictions of critical detonation initiation energy based on detonation-velocity curvature laws. In particular, we find that for a main reaction layer of fixed length, the initiation energy increases as the length of the induction layer increases. In the context of a three-step chain-branching model previously studied by Short & Quirk (1997), the energy required to initiate a detonation would increase as the chain-branching cross-over temperature increased. Finally some calculations that illustrate the important effect that arclength and transverse flow variations may have on the steady propagation of non-planar detonation fronts were conducted, in particular for some rate-stick calculations where the detonation velocity was shown to vary significantly with arclength. This is in contrast to the previous theories of detonation shock dynamics where the detonation velocity was purely a function of the shock curvature to leading order. However, such significant variation of the detonation velocity with arclength has been observed, for example, in recent unpublished rate-stick calculations on the explosive ANFO, ammonium nitrate and fuel oil, and work is currently being conducted to fit the observed variations to the propagation law (4.25).

Finally, we note that an important extension of the current work is to investigate the stability of the steady propagation laws derived here, and to construct appropriate time-dependent evolution laws when they are unstable, as in Short (2001) for the one-dimensional case. In general, though, this is a difficult task due to the large number of limiting cases that need to be investigated. For the two-component reaction model, the underlying steady wave can have three limiting forms, namely an induction one that is shorter, of the same order as, or longer than the main reaction zone layer. Additionally, there are many possible scales for the curvature of the shock front, which may or may not influence the induction and main reaction layer structures, depending on their relative scale. However, some form of (4.25) should contain the leading-order steady structure in all these cases. Such a study is currently in progress.

M. S. was funded by the AFOSR and DOE LANL.

Appendix. Reactive-Euler equations

Using intrinsic, shock-based, Bertrand coordinates, the compressible reactive Euler equations are given by

mass:

$$(\rho U_n)_{,n} = -\omega\mu\frac{\kappa\rho(U_n + D_n)}{1 + \omega\mu n\kappa} - \mu^2\frac{(\rho u_\xi)_{,\xi}}{1 + \omega\mu n\kappa} - \mu\left(\omega B + \frac{\mu n D_{n,\xi}}{1 + \omega\mu n\kappa}\right)\rho_{,\xi}, \qquad (A\,1)$$

n-momentum:

$$U_n U_{n,n} + \frac{1}{\rho} p_{,n} = -\mu\left(\omega B + \mu \frac{u_\xi + n D_{n,\xi}}{1 + \omega\mu n\kappa}\right)\left(U_{n,\xi} + D_{n,\xi}\right) + \frac{\mu^3 \omega u_\xi^2 \kappa}{1 + \omega\mu n\kappa} - \mu^2 \frac{u_\xi D_{n,\xi}}{1 + \omega\mu n\kappa}, \quad \text{(A 2)}$$

ξ-momentum:

$$U_n u_{\xi,n} = -\frac{p_{,\xi}}{\rho(1 + \omega\mu n\kappa)} - \mu\left(\omega B + \mu \frac{u_\xi + n D_{n,\xi}}{1 + \omega\mu n\kappa}\right) u_{\xi,\xi} - (U_n + D_n)\frac{\omega\mu\kappa u_\xi - D_{n,\xi}}{1 + \omega\mu n\kappa}, \quad \text{(A 3)}$$

energy:

$$U_n e_{,n} - \frac{p}{\rho^2} U_n \rho_{,n} = -\mu\left(\omega B + \mu \frac{u_\xi + n D_{n,\xi}}{1 + \omega\mu n\kappa}\right)\left(e_{,\xi} - \frac{p}{\rho^2}\rho_{,\xi}\right), \quad \text{(A 4)}$$

reaction:

$$U_n \lambda_{i,n} = r_i - \mu\left(\omega B + \mu \frac{u_\xi + n D_{n,\xi}}{1 + \omega\mu n\kappa}\right) \lambda_{i,\xi}, \quad \text{(A 5)}$$

for density ρ, pressure p, normal velocity U_n, transverse velocity u_ξ, specific internal energy e, reaction progress variable for the ith reaction λ_i with rate r_i. The parameters ω and μ are defined as the shock angle scale and arclength scale respectively.

REFERENCES

Aslam, T. D., Bdzil, J. B. & Hill, L. G. 1998 Extensions to DSD theory: Analysis of PBX9502 rate stick data. In *Eleventh Symposium* (*Intl*) *on Detonation*. Office of Naval Research, p. 21–29.

Aslam, T., Bdzil, J. B. & Stewart, D. S. 1996 Level set methods applied to modeling detonation shock dynamics. *J. Comput. Phys.* **126**, 390–409.

Bdzil, J. B. 1981 Steady state two-dimensional detonation. *J. Fluid Mech.* **108**, 185–226.

Bdzil, J. B. 2000 Detonation front models: theories and methods. Preprint.

Bourlioux, A. & Majda, A. J. 1992 Theoretical and numerical structure for unstable two-dimensional detonations. *Combust. Flame* **90**, 211–229.

Buckmaster, J. D. 1989 A theory for triple point spacing in overdriven detonation waves. *Combust. Flame* **77**, 219–228.

Eckett, C. A., Quirk, J. J. & Shepherd, J. E. 2000 The role of unsteadiness in direct initiation of gaseous detonations. *J. Fluid Mech.* **421**, 147–183.

Fickett, W. & Davis, W. C. 1979 *Detonation*. University of California Press.

He, L. & Clavin, P. 1994 On the direct initiation of gaseous detonations by an energy source. *J. Fluid Mech.* **277**, 227–248.

Kailasanath, K., Gardner, J. H., Boris, J. P. & Oran, E. S. 1991 Numerical simulations of unsteady reactive flows in a combustion chamber. *Combust. Flame* **86**, 115–134.

Klein, R. 1991 On the dynamics of weakly curved detonations. *IMA Maths Applics.* **35**, 127–166.

Klein, R. 1994 Curved detonations in explosive gas mixtures with high temperature sensitivity. Preprint.

Klein, R., Krok, J. C. & Shepherd, J. E. 1994 Investigation of curved quasi-steady detonations using asymptotic analysis and detailed chemical kinetics. Preprint.

Klein, R. & Stewart, D. S. 1993 The relation between curvature, rate state-dependence and detonation velocity. *SIAM J. Appl. Maths* **53** 1401–1435.

Korobeinikov, V. P. 1991 Problems of Point-Blast Theory. American Institute of Physics.

Lee, J. H. S. & Higgins, A. J. 1999 Comments on criteria for direct initiation of detonation. *Phil. Trans. R. Soc. Lond.* A **357**, 3503–3521.

Oran, E. S., Jones, D. A. & Sichel, M. 1992 Numerical simulations of detonation transmission. *Proc. R. Soc. Lond.* A **436**, 267–297.

Oran, E. S. & Boris, J. P. 1987 *Numerical Simulation of Reactive Flow*. Elsevier.

Sharpe, G. J. 2000*a* The effect of curvature on pathological detonations. *Combust. Flame* **123**, 68–81.

Sharpe, G. J. 2000*b* The structure of planar and curved detonation waves with reversible reactions. *Phys. Fluids* A **12**, 3007–3020.

Sharpe, G. J. 2001 Transverse waves in numerical simulations of cellular detonations. *J. Fluid Mech.* **447**, 31–51.

Sharpe, G. J. & Falle, S. A. E. G. 2000 Two-dimensional numerical simulations of idealized detonations. *Proc. R. Soc. Lond.* A **456**, 2081–2100.

Short, M. 2001 A nonlinear evolution equation for pulsating Chapman–Jouguet detonations with chain-branching kinetics. *J. Fluid Mech.* **430**, 381–400.

Short, M., Kapila, A. K. & Quirk, J. J. 1999 The hydrodynamic mechanisms of pulsating detonation wave instability. *Phil. Trans. R. Soc. Lond.* A **357**, 3621–3628.

Short, M. & Quirk, J. J. 1997 On the nonlinear stability and detonability limit of a detonation wave for a model three-step chain-branching reaction. *J. Fluid Mech.* **339**, 89–119.

Short, M., Sharpe, G. S. & Bdzil, J. B. 2001 Curved detonations with three-step chain-branching kinetics, in preparation.

Short, M. & Stewart, D. S. 1998 Cellular detonation stability. Part 1. A normal-mode linear analysis. *J. Fluid Mech.* **368**, 229–262.

Stewart, D. S. & Bdzil, J. B. 1988*a* *A Lecture on Detonation Shock Dynamics*. Lecture Notes in Physics, vol. 299, pp. 17–30. Springer.

Stewart, D. S. & Bdzil, J. B. 1988*b* The shock dynamics of stable multidimensional detonation. *Combust. Flame* **72**, 311–323.

Taylor, G. I. 1950 The formation of a blast wave by a very intense explosion. I. Theoretical discussion. *Proc. R. Soc. Lond.* A **201**, 159–528.

Yao, J. & Stewart, D. S. 1995 On the normal shock velocity-curvature relationship for materials with large activation energy. *Combust. Flame* **100**, 519–528.

Yao, J. & Stewart, D. S. 1996 On the dynamics of the multi-dimensional detonation. *J. Fluid Mech.* **309**, 225–275.